

Synthesis and Characterization of Novel Nanomaterials for Removal of Textile Dyes in Industrial Wastewater

Leshan Usgodaarachchi

MP20700324

MPhil in Materials Engineering

Department of Materials Engineering


Sri Lanka Institute of Information Technology

February 2022

Declaration

I hereby declare that to the best of my knowledge this submission is my own work and it neither contains direct material previously published nor written by another person or material which to substantial extent has been accepted for the award of any other academic qualification of a university or other institute of higher learning except where acknowledgement is made in the text.

Certified by

Signature : 

Date : 5/2/2022

Name of Supervisor I : Dr. Charitha Jayaruk

Signature :

Date :

Name of Supervisor II : Dr. Mudith Karunaratne

Signature :

Date :

Name of Supervisor III : Prof. Saravanamuthu Vigneswaran

Signature :

Date :

ACKNOWLEDGEMENT

Foremost, I would like to express my deepest gratitude to my supervisor, Dr. Charitha Thambiliyagodage and my co-supervisors Prof. Saravanamuthu Vigneswaran and Dr. Mudith Karunaratne for proper guidance, encouragement, motivation, and continuous support for the successful completion of the research and the thesis. All of the work succeeded because of their kindness and excellent supervision.

The opportunity provided to me by Dr. Charitha Thambiliyagodage for working as Research assistant on his Accelerating Higher Education Expansion and Development (AHEAD) project driven me into gain my special curiosity in wide range of topics in materials science and engineering. Specially, the condensed matter, catalysts, solid-state materials, supercapacitors, graphene-based materials, metal-organic frameworks (MOF), zero-valent metal composites, heterogeneous material designing, topology and morphology-controlled synthesis of nanomaterials, electronic, optical, and magnetic materials (EOM) materials and high energy materials. Also, the freedom and free mind set given to myself by Dr. Charitha Thambiliyagodage resulted to expand the scope of this research work. Furthermore, I would like to express my sincere gratitude to Prof. Saravanamuthu Vigneswaran for effort in review & editing our articles prior submissions to journals. I am most privileged to convey my gratitude to my colleges for the immense support throughout various aspects of the research work. I would like to thank the World Bank Project for funding my research project and Sri Lanka Institute of Nanotechnology (SLINTEC), Industrial Technology Institute (ITI), University of Moratuwa and University of Peradeniya for providing instrumental facilities in materials characterization.

ABSTRACT

Inefficient treatments and uncontrolled pollutants generation to the environment has been significantly affected the living standards in the ecosphere. The advancement in nanotechnology resulted in the effective treatment of all of the pollutants generated in the environment. In the field of textile dye removal, the special features of nanomaterials are gaining attention due to their enhanced physical, chemical and mechanical properties. Rice husk is an agricultural waste material that is used for the production of adsorbents in this study. Mesoporous silica nanoparticles were successfully synthesized by using rice husk as the raw material via a sol-gel pathway using cetyltrimethylammonium bromide (CTAB) as the structure-directing agent. The functionalization of silica nanoparticles was taken place in two pathways, such as in-situ and post functionalization methods by using 3-aminopropyltriethoxysilane (APTES) as the functionalization agent. Mesoporous silica nanoparticles were able to effectively adsorb methylene blue dye from aqueous solutions. The adsorption of MB could be best described by the pseudo-second-order model and well fitted to the Langmuir equation, with a maximum monolayer capacity of 19.26 mg/g. Photocatalytic decomposition of the organic pollutants gains emerging attention after the discovery of water splitting ability by TiO_2 . The high purity (98.8%, TiO_2) rutile nanoparticles were successfully synthesized using ilmenite sand as the initial titanium source. This novel synthesis method was cost-effective and straightforward due to the absence of the traditional gravity, magnetic, electro statistic separation, ball milling and smelting processes. Also, highly corrosive environmentally hazardous acid leachate generated during the leaching process of ilmenite sand was effectively converted into highly efficient photocatalysts. The most efficient photocatalysts were composed of anatase- TiO_2 /rutile- $\text{TiO}_2/\text{Fe}_2\text{O}_3$, $\alpha\text{-Fe}_2\text{O}_3/\text{Fe}_2\text{TiO}_5/\text{TiO}_2$ and $\text{Fe}_2\text{TiO}_5/\text{TiO}_2$. The synthesized nanocomposites were characterized by microscopic (SEM and TEM) and spectroscopic (XRD, Raman, XPS, FT-IR and DRS) analytical techniques. These nano heterostructures were catalytically active for the photodegradation of methylene blue upon irradiation by a light source (LED or sunlight). Efficient charge separation and limiting electron-hole recombination in photocatalyst surfaces resulted in the overall performance of synthesized material. Reduced

graphene oxide (r-GO) has lately attracted a lot of attention to overcome limitations associated with photocatalysts. The honeycomb sp^2 network structure of r-GO improves charge separation and transportation through the surface of the catalyst. The fabricated GO/Fe₃O₄ heterogeneous photocatalyst shows very efficient degradation performance by overcoming the limitations associated with the narrow bandgap of Fe₃O₄ (0.1 eV). Finally, the synthesis of graphene like materials by catalytic graphitization of sucrose by using Fe and Ti transition metals studied in this study. Herein, we reported that Fe and Ti metal oxides promoted to the graphitization process at low temperature. Sucrose mixed with only uncalcined Fe₂O₃ produced Fe₃C, Fe, Fe₃O₄ dispersed on graphitic carbon, while sucrose mixed with only Fe₂TiO₅/TiO₂ product, and mixed with uncalcined Fe₂O₃ and Fe₂TiO₅/TiO₂ led to the production of TiO₂, Fe₃C, Fe, Fe₃O₄ dispersed on graphitic carbon. The most outstanding photocatalyst synthesized material composed with TiO₂/Fe₃C/Fe/Fe₃O₄–Graphitic carbon which is sun light sensing photocatalyst.

Keywords: Heterostructures, Rice husk, Reduced graphene oxide, Photocatalysis, Catalytic graphitization, Ilmenite sand

Table of Contents

ACKNOWLEDGEMENT	ii
ABSTRACT.....	iii
Table of Contents	v
List of Tables	viii
List of Figures	ix
Abbreviations	xiii
CHAPTER 1: INTRODUCTION	1
1.1 Problem Statement	2
1.2 Research gap.....	3
CHAPTER 2: LITERATURE REVIEW	10
2.1 Chemistry of dyes.....	11
2.2 Classification of dyes	11
2.2.1 Direct dyes	12
2.2.2 Reactive dye.....	13
2.2.3 Vat dyes	13
2.2.4 Disperse dyes	14
2.2.5 Azo Dyes	15
2.3 Wastewater Treatment.....	16
2.3.1 Physicochemical techniques	17
2.3.2 Chemical oxidation techniques.....	19
2.4 Adsorption of Dyes on Silica nanomaterials	24
2.5 Synthesis of Titanium dioxide from natural Ilmenite sand	27
2.5.1 Sulphate Process	28
2.5.2 Chloride Process	29
2.6 Titanium Dioxide	30
2.7 TiO ₂ based photocatalysts and enhancement of the photocatalytic activity of TiO ₂	33
2.7.1 Fundamentals of photocatalysis.....	33
2.7.2 Metal modified TiO ₂	35
2.7.3 Non-metal modified TiO ₂	37
2.7.4 Semiconductors coupling TiO ₂ and heterojunction construction	37
2.7.5 Graphene-based photocatalysts	39
CHAPTER 3: METHODOLOGY	41
3.1 Synthesis of mesoporous silica nanoparticles derived from rice husk and surface-controlled amine functionalization for efficient adsorption of methylene blue from aqueous solution	41
3.1.1 Materials	41

3.1.2 Washing and acid treatment.....	41
3.1.3 Thermal treatment.....	42
3.1.4 Preparation of the silica precursor	42
3.1.5 Preparation of mesoporous silica nanoparticles by sol-gel pathway (MSN-A).....	42
3.1.6 Amine functionalization of silica nanoparticles	43
3.1.7 Characterization of materials	43
3.2 Fabrication of TiO ₂ and visible light sensitive titanium-iron based photocatalysts from natural ilmenite	44
3.2.1 Materials	44
3.2.2 Hydrochloric acid leaching and facile separation.....	44
3.2.3 Preparation of Nanomaterials	45
3.2.4 Materials Characterization.....	47
3.3 Efficient photodegradation activity of α -Fe ₂ O ₃ /Fe ₂ TiO ₅ /TiO ₂ and Fe ₂ TiO ₅ /TiO ₂ nanocomposites synthesized from natural ilmenite.....	48
3.3.1. Materials and methods.....	48
3.3.2 Synthesis of Fe ₂ TiO ₅ /TiO ₂	48
3.3.3 Synthesis of α -Fe ₂ O ₃ /Fe ₂ TiO ₅ /TiO ₂	48
3.3.4 Synthesis of α -Fe ₂ O ₃	49
3.3.5 Characterization methods	49
3.3.6 Photocatalytic activity	50
3.4 Photocatalytic activity of GO/Fe ₃ O ₄ fabricated by Sri Lankan graphite under visible light irradiation	50
3.4.1 Materials	50
3.4.2 Synthesis of Graphene Oxide (GO).....	50
3.4.3 Synthesis of Fe ₃ O ₄ nanoparticles.....	51
3.4.4 Synthesis of GO/Fe ₃ O ₄	51
3.4.5 Photocatalytic activity evaluation.....	51
3.5 Efficient photocatalysis of TiO ₂ /Fe ₃ C/Fe/Fe ₃ O ₄ – Graphitic carbon composites fabricated by catalytic graphitization of sucrose using natural ilmenite under visible light.....	52
3.5.1 Materials	52
3.5.2 Preparation of Nanomaterials	52
3.5.3 Antibacterial activity	53
3.5.4 Characterization	55
Chapter 4: Results and Discussion.....	56
4.1 Synthesis of mesoporous silica nanoparticles derived from rice husk and surface-controlled amine functionalization for efficient adsorption of methylene blue from aqueous solution	56
4.1.1 SEM Analysis	58
4.1.2 FTIR Analysis.....	59
4.1.3 TGA Analysis	60
4.1.4 BET Analysis.....	61
4.1.5 Adsorption Kinetics	63
4.1.6 Adsorbent material optimization	63
4.1.7 pH parameter optimization	64

4.1.8 Adsorbent dosage parameter optimization	65
4.1.9 Adsorption kinetics modelling.....	66
4.1.10 Adsorption Isotherms.....	71
4.2 Fabrication of TiO ₂ and visible light sensitive titanium-iron based photocatalysts from natural ilmenite	77
4.2.1 Precipitation of the rutile nanoparticles and photocatalyst composites	77
4.2.2 XRD and XRF Analysis	80
4.2.3 Raman analysis	84
4.2.4 SEM morphological analysis.....	85
4.2.5 Nitrogen sorption analysis	86
4.2.6 Optical adsorption properties.....	88
4.2.7 Photocatalytic degradation.....	88
4.3 Efficient photodegradation activity of α -Fe ₂ O ₃ /Fe ₂ TiO ₅ /TiO ₂ and Fe ₂ TiO ₅ /TiO ₂ nanocomposites synthesized from natural ilmenite.....	95
4.3.1 XRD and XRF Analysis	95
4.3.2 Raman analysis	98
4.3.3 Morphological analysis.....	100
4.3.4 XPS Analysis	102
4.3.5 DRS analysis.....	104
4.3.6 Photocatalytic activity	104
4.4 Photocatalytic activity of GO/Fe ₃ O ₄ fabricated by Sri Lankan graphite under visible light irradiation	108
4.4.1 SEM analysis	108
4.4.2 XRD analysis	109
4.4.3 FT-IR spectroscopic analysis.....	110
4.4.4 Magnetic behavior	111
4.4.5 Photocatalytic activity	112
4.5 Efficient photocatalysis of TiO ₂ /Fe ₃ C/Fe/Fe ₃ O ₄ – Graphitic carbon composites fabricated by catalytic graphitization of sucrose using natural ilmenite under visible light.....	114
4.5.1 XRD Analysis.....	114
4.5.2 TEM analysis.....	118
4.5.3 SEM analysis	120
4.5.4 Resonant Raman Spectroscopy.....	122
4.5.5 XPS Analysis	126
4.5.6 XRF analysis.....	128
4.5.7 DRS analysis.....	128
4.5.8 Photocatalysis performance	131
4.5.9 Antibacterial activity	136
CONCLUSION	138
REFERENCES	142

List of Tables

Table 1. 1. Comparative analysis of the existing water treatment methods	23
Table 1. 2. Methods for reducing contamination by improving characteristics of RHA	26
Table 4. 1. Textural parameters of MSN-A and functionalized silica materials	61
Table 4. 2. Adsorption kinetic parameters of methylene blue onto MSN.....	71
Table 4. 3. Parameters calculated by Langmuir Freundlich and Temkin adsorption isotherm models	76
Table 4. 4. Chemical composition of the ilmenite sand as metallic oxides.....	80
Table 4. 5. Structural properties of the composite analyzed by XRD crystalline planes	83
Table 4. 6. Textural characteristics of TiO ₂ samples as prepared.....	87
Table 4. 7. Dark adsorption of methylene blue onto nanocomposites: kinetic factors	90
Table 4. 8. Linear and polynomial kinetic parameters for visible light photocatalysis.....	92
Table 4. 9. Organic dye degradation rates using photocatalysts based on ilmenite sand	94
Table 4. 10. XRD analysis of the composites' structural properties.....	96
Table 4. 11. XRF analysis of ilmenite sand and FFT-800	97
Table 4. 12. Initial rate constants of the photodegradation of MB by the composites	106
Table 4. 13. Metallic composition of the synthesized materials as metallic oxides	128
Table 4. 14. Percentage adsorption removal of MB, adsorption capacity and the rate constant of MB degradation by the synthesized materials.....	131
Table 4. 15. A comparison of the obtained adsorption capacities with the same reported in the literature	134
Table 4. 16. Antibacterial Assay	137

List of Figures

Figure 2. 1. Systematic illustration of Direct Fast Brown M and Brilliant Yellow	12
Figure 2. 2. Systematic illustration of Reactive blue 4 and Reactive blue 19	13
Figure 2. 3. Systematic illustration of Vat violet 10 and Vat blue 4.....	14
Figure 2. 4. Systematic illustration of Disperse Violet 28 and disperse yellow 9	15
Figure 2. 5. Systematic illustration of Pigment yellow 3 and Pigment red 122	16
Figure 2. 6. Crystalline structure of Anatase (left) Rutile (middle) and Brookite (right)	31
Figure 2. 7. (a) Anatase [TiO ₆] and (b) Anatase unit cell	32
Figure 2. 8. (a) Ball and stick models of the basic rutile [TiO ₆] octahedron and (b) tetragonal unit cell of rutile	32
Figure 2. 9. The method of photocatalytic water splitting for H ₂ production	34
Figure 2. 10. (a) Charge transfer diagram for metal/TiO ₂ under UV light irradiation due to the Schottky junction; (b) Charge transfer diagram for metal/TiO ₂ under visible light irradiation due to surface plasmon resonance (SPR) effects.....	36
Figure 2. 11. The effects of N and S dopants on TiO ₂ improved visible light photocatalytic activity	37
Figure 2. 12. Photoactivation and charge carriers transferring according to the Type I and Type II band alignments	38
Figure 2. 13. (a) The SP ² hybridization between carbon atoms and (b) honeycomb structural arrangement of graphene.....	40
Figure 3. 1. Refluxing of Rice husk in 10% hydrochloric acid.....	35
Figure 3. 2. (a) Acid leached rice husk inside the muffle furnace prior combustion and (b) Acid leached rice husk ash	42
Figure 3. 3. (a) Sol-gel synthesized silica nanoparticles and (b) Facile separation of synthesized MSN	43
Figure 3. 4. (a) Conc hydrochloric acid refluxing process of ilmenite sand (b) Facile separated ilmenite sand acid leachate and (c) separated iron chloride titanium residue and un-leached ilmenite sand	45
Figure 3. 5. (a) Graphene oxide suspension and (b) Graphene oxide films	51

Figure 4. 1. XRD patterns of RHA and Acid leached RHA...	50
Figure 4. 2. (a) RHA and (b) acid leached RHA.....	57
Figure 4. 3. The mechanism of formation of mesoporous silica spheres.....	58
Figure 4. 4. SEM images of the (a) MSN-A (b) MSN-B (c) MSN-C and (d) MSN-D.....	59
Figure 4. 5. (a) FTIR spectra of MSN-A and amine-modified silica particles (b) FTIR spectra of MSN-A and amine-modified silica particles responsible for amine vibration bands.....	59
Figure 4. 6. TGA curves for MSN-A and amine-modified silica nanoparticles	61
Figure 4. 7. (a) Nitrogen adsorption-desorption isotherms of MSN-A and amine-modified silica nanoparticles. (b) Pore size distribution of MSN-A and amine-modified silica nanoparticles.	62
Figure 4. 8. Performance of MSN-A MSN-B MSN-C and MSN-D adsorbents on adsorption of MB	64
Figure 4. 9. Effect of pH on adsorption of MB on MSN-A MSN-B MSN-C and MSN-D adsorbents.....	65
Figure 4. 10. (a) The percentage removal of MB on different weight of MSN-A loading and (b) Effect of MSN-A dosage on MB adsorption capacity.....	66
Figure 4. 11. Pseudo first order kinetics model for adsorption of MB on to MSN	69
Figure 4. 12. Pseudo second order kinetics model for adsorption of MB on to MSN	71
Figure 4. 13. Langmuir adsorption isotherm model of MB on to MSN-A.....	73
Figure 4. 14. Freundlich adsorption isotherm model of MB on to MSN-A	74
Figure 4. 15. Temkin adsorption isotherm model of MB on to MSN-A	76
Figure 4. 16. (a) Facilely separated unreacted ilmenite leached titanium residue and leached iron chloride with other metallic chlorides and (b) $\text{Na}_x\text{TiO}_y(\text{OH})_j$ titanium solution (Titanium-sol)	77
Figure 4. 17. XRD pattern of (a) natural ilmenite (b) dried titanium residue (c) amorphous titanium dried at 100 °C (d) TiO_2 -A (e) TiO_2 -B (f) uncalcined TFTO ($\text{TiO}_2/\text{Fe}_2\text{O}_3$) composite (g) TFTO-800 composite (h) TF composite (i) TF-450 composite and (j) TF-800 composite	81

Figure 4. 18. Raman pattern of (a) TFTO-800 (b) TF-450 (c) TF-800 and (d) TiO ₂ -A.....	85
Figure 4. 19. SEM images of (a) Ilmenite sand (b) TiO ₂ -A (c) TiO ₂ -B (d) uncalcined TF composite (e) TF-450 composite and (f) TF-800 composite	86
Figure 4. 20. (a) Nitrogen adsorption-desorption isotherms of TiO ₂ -A and TiO ₂ -B (b) pore size distribution of TiO ₂ -A and TiO ₂ -B	87
Figure 4. 21. (a) Kubelka-Munk function vs wavelength plot for TiO ₂ -A Tauc Plot for determination of (b) direct band gap (n = 1/2)	88
Figure 4. 22. (a) MB degradation rate at various time intervals (b) TFTO-800 TF-450 and TF-800 pseudo first order models Dark 60 min adsorption of MB onto produced nanocomposite (c) pseudo second order model of TF-450 and (d) pseudo second order model of TFTO-800 and TF-800.....	90
Figure 4. 23. Decolorization of MB by photocatalytic decolorization.....	91
Figure 4. 24. First order kinetic photodegradation of MB under LED Light for (a) TFTO-800 (b) TF-450 and (c) TF-800 nanocomposites.....	92
Figure 4. 25. XRD patterns of (a) F00-600 (b) FF0-600 (c) FFT-600 (d) F00-800 (e) FT0-800 (f) FFT-800 and (g) TiO ₂ -800	97
Figure 4. 26. Raman spectra of (a) F00-600 (b) FF0-600 (c) FFT-600 (d) F00-800 (e) FT0-800 (f) FFT-800 and (g) TiO ₂ -800	99
Figure 4. 27. (a) Bright field TEM image (b) (c) HRTEM images of FFT-600 (d) (e) HRTEM image of FFT-800 EDX spectra of FFT-600 (f) composite (g) C (h) O I Ti (j) Fe EDX spectra of FFT-800 (k) composite (l) C (m) O (n) Ti and (o) Fe EDX spectra of FFT-600.....	101
Figure 4. 28. SEM images of (a) FFT-600 (b) FFT-800.....	102
Figure 4. 29. High resolution XPS spectra of (a) Ti 2p of FFT-600 (b) Ti 2p of FFT-800 (c) Fe 2p of FFT-600 (d) Fe 2p of FFT-800 (e) C 1s and (f) O 1s of FFT-800 Survey spectra of (g) FFT-600 (h) FFT-800	103
Figure 4. 30. DRS spectra of (a) TiO ₂ (b) F00-800 (c) FT0-800 (d) FFT-800 .	104
Figure 4. 31. Photocatalytic efficiency of different catalysts towards degradation of MB on exposure to (a) LED source (b) Sunlight.....	106
Figure 4. 32. SEM images of (a) (b) GO (c) GO/Fe ₃ O ₄ and (d) GO/Fe ₃ O ₄ obtained by secondary electron detector and backscatter electron detector respectively	109

Figure 4. 33. XRD patterns of (a) natural graphite powder (b) GO (c) Fe ₃ O ₄ and (d) GO/Fe ₃ O ₄	110
Figure 4. 34. FT-IR spectra of GO Fe ₃ O ₄ and GO/Fe ₃ O ₄	111
Figure 4. 35. (a) GO/Fe ₃ O ₄ with degraded MB after the reaction (b) magnetic GO/Fe ₃ O ₄ attached to an external magnet	112
Figure 4. 36. (a) Rate plot (b) variation of C/C ₀ with time (c) conversion of MB at each cycle showing the reusability of the GO/Fe ₃ O ₄	113
Figure 4. 37. XRD patterns of (a) precursor compounds (b) SF composites (c) SI composites (d) SFI composites.	117
Figure 4. 38. Bright field TEM images of (a) SF 10 (b) SI 10 (c) SFI 20, HRTEM images of (d) SI 10 (e) and (f) SF 2.5 (g) SI 10 (h), (i) and (j) SFI 20, Selected area diffraction patterns of (k) SF 2.5 (l) SI 10 (m) SFI 20.....	119
Figure 4. 39. SEM images of (a), (b) SF 10 (c), (d) SF 1 (e), (f) SI 10 (g), (h) SI 1 (i), (j) SFI 20 (k), (l) SFI 2, EDX spectra of (m) SF 10 (n) SF 1 (o) SI 10 (p) SI 1 (q) SFI 20 (r) SFI 2.....	121
Figure 4. 40. (a) Peak deconvolution of SF 10, variation of I _D /I _G of (b) SF (c) SI and (d) SFI composites, variation of L _a of (e) SF (f) SI and (g) SFI composites, variation of L _D of (h) SF (i) SI and (j) SFI composites, 1/L _D ² vs. L _a ² of (k) SF (l) SI and (m) SFI	125
Figure 4. 41. High resolution spectra of C 1s of (a) amorphous carbon (b) α-Fe ₂ O ₃ (c) FTO, high resolution spectra of O 1s of (d) amorphous carbon (e) α-Fe ₂ O ₃ (f) FTO, high resolution spectra of Fe 2p of (g) FTO (h) α-Fe ₂ O ₃ (i) SF 10 (j) SF 1 (k) SI 10 (l) SI 1 (m) SFI 20 (n) SFI 2, high resolution spectra of Ti 2p of (o) FTO (p) SI 10 (q) SI 10 (r) SFI 20 and (s) SFI 2	127
Figure 4. 42. (a) Diffuse reflectance UV-Visible spectra (b) direct transition (c) indirect transition of the synthesized composites	130
Figure 4. 43. First order kinetics plots of (a) SF (b) SI (c) SFI composites	136

Abbreviations

MSN	Mesoporous silica nanoparticles
CTAB	Cetyltrimethylammonium bromide
APTES	3-Aminopropyltriethoxysilane
RH	Rice husk
RHA	Rice husk ash
MSN-A	Mesoporous silica nanoparticles by sol-gel pathway
MSN-B	Amine modified MSN via co-synthesis method by pre addition of APTES
MSN-C	Amine modified MSN via co-synthesis method by post addition of APTES
MSN-D	Amine modified MSN via post grafting method
TiO ₂ -A	800 °C annealed amorphous TiO ₂
TiO ₂ -B	800 °C annealed CTAB assigned amorphous TiO ₂
TFTO	Uncalcined TiO ₂ /Fe ₂ TiO ₅
TFTO-800	800 °C annealed TFTO powder TFTO
TF	Uncalcined TiO ₂ /Fe ₃ O ₄
TF-450	450 °C annealed TF powder
TF-800	800 °C annealed TF powder
FFO-600	600 °C annealed Fe ₂ TiO ₅ /TiO ₂
FOO-600	600 °C annealed α-Fe ₂ O ₃
FOO-800	800 °C annealed α-Fe ₂ O ₃
SF	Carbon and Iron composite

SI	Carbon and Ilmenite composite
SIF	Carbon, Ilmenite and Iron composite
LED	Light eliminative diode
r-GO	Reduced graphene oxide
GO	Graphene Oxide
SPR	Surface plasmon resonance
LSR	Localized surface plasmon resonance
DET	Direct electron transfer
FE-SEM	Field Emission Scanning Electron Microscope
FTIR	Fourier Transformation Infrared Spectroscopy
TGA	Thermogravimetric analysis
XRD	X-ray diffraction
XRF	X-ray fluorescence analyzer
XPS	X-ray photoelectron spectroscopy
TEM	Transmission electron microscopy
EDS	Energy dispersive spectra
DI	Deionized water
AHEAD	Accelerating Higher Education Expansion and Development
MOF	Metal-organic frameworks
EOM	Electronic, optical, and magnetic materials
SLINTEC	Sri Lanka Institute of Nanotechnology
ITI	Industrial Technology Institute